TECHNICAL NOTE SUBMITTED TO 'GÉOTECHNIQUE'

DATE:

13/02/2018

TITLE:

Enhancement of bearing capacity from consolidation: due to changing strength or failure mechanism?

AUTHOR:

Stanier, S.A.* and White, D.J.**

POSITION AND AFFILIATION:

* Research Fellow – Centre for Offshore Foundation Systems, University of Western Australia.
** Professor – Centre for Offshore Foundation Systems, University of Western Australia.

CONTACT ADDRESS:

Centre for Offshore Foundation Systems
M053 Fairway
Crawley
WA 6009
Australia

NUMBER OF WORDS, FIGURES AND TABLES:

Words: 2446
Figures: 7
Tables: 1

KEYWORDS:

Consolidation, bearing capacity, footings/foundations, shear strength, numerical modelling.

ENHANCEMENT OF BEARING CAPACITY FROM CONSOLIDATION: DUE TO CHANGING STRENGTH OR FAILURE MECHANISM?

Stanier, S.A. & White, D.J.

ABSTRACT

Bearing capacity of shallow foundations is higher following preload (or self-weight)-induced consolidation because the soil strength changes, and perhaps because the failure mechanism changes. Previous studies have illustrated this effect by plotting or predicting changes in either bearing capacity factor or strength. This study explores the relative contribution of these two effects. This is achieved by formalising a definition of bearing capacity factor, which is described in terms of the average strength mobilised in the deformation mechanism at failure. Using the alternative definition of bearing capacity factor, the gain in foundation capacity is shown to be almost entirely due to changes in soil strength, rather than bearing capacity factor, which remains largely unaffected by the strength gains. This observation should encourage future studies into consolidated bearing capacity to present gains in capacity in terms of changes in mobilised strength rather than changes in bearing capacity factors, and supports the use of prediction methods that focus on defining the change in soil strength.

INTRODUCTION

When a foundation is placed on soft clay, the self-weight or sustained vertical load causes consolidation of the soil, resulting in an increase in the bearing capacity of the foundation over time. Prediction and utilisation of this gain in bearing capacity allows more efficient foundation design. Previous studies have observed this behaviour via model-scale experiments (Lehane & Gaudin, 2005; Bienen & Cassidy, 2013; Stanier et al. 2014; Vulpe & White, 2014; Vulpe et al. 2016a,b), numerical simulations (Bransby, 2002; Zdravkovic et al. 2003, Gourvenec et al. 2014; Fu et al. 2015; Feng and Gourvenec, 2016), and field tests (Lehane & Jardine, 2003; Gaone et al. 2017).

For a simple plane strain shallow foundation on normally consolidated fine grained soil (Figure 1) the ultimate bearing capacity, V_u, is linked to the in situ soil strength via a bearing capacity factor, N_{cV}, defined as:

$$N_{cV} = \frac{V_u}{Bs_{um}} \approx f\left(\frac{kB}{s_{um}}\right) \quad 1$$

where B is the footing width, s_{um} is the undrained strength at the mudline and k is the gradient of strength with depth. The bearing capacity factor is often given as a function of the dimensionless parameter, kB/s_{um}, which describes the uniformity of the soil strength with depth. For horizontal and moment loading we can define similar capacity factors as follows:

$$N_{cH} = \frac{H_u}{Bs_{um}} \quad 2$$

$$N_{cM} = \frac{M_u}{B^2 s_{um}} \quad 3$$

If the foundation is subjected to a maintained preload, V_p, (where $V_p < V_u$) excess pore pressure is initially created. This pore pressure dissipates, leading to consolidation and varying levels of strength gain in the surrounding soil. This change in strength distribution

causes a gain in foundation bearing capacity, which can be linked to two potential effects: (i) the increase in the undrained strength, s_u, of the soil that fails when the bearing capacity is reached and (ii) a change in the deformation mechanism at failure due to the change in distribution of soil strength beneath the foundation. In developing methods to predict the increase in foundation capacity due to preloading some researchers describe modifications to the bearing capacity factor and use the in-situ strength profile (e.g. Bienen & Cassidy, 2013; Stanier et al. 2014) whilst others have framed the behavior as a change in the strength (e.g. Gourvenec et al. 2014; Feng & Gourvenec, 2015). To develop simple prediction tools for changing bearing capacity, it is useful to understand the relative importance of these two effects so as to rationalise which is the most appropriate approach, and focus attention on the controlling aspect of the behaviour.

This technical note tackles this uncertainty by separating the two effects via a specific definition of the bearing capacity factor that links it to the deformation mechanism. This allows the separate effects of the changing soil strength and the changing failure mechanism to be quantified explicitly.

DEFINITION OF BEARING CAPACITY FACTOR, N_C

A definition for the bearing capacity factor, N_c, is now introduced to distinguish the effects of soil strength and failure mechanism in numerical analyses. Instead of using the in-situ mudline strength, s_{um}, in the normalisation of bearing capacity (Equations 1-3), we use the average mobilised undrained strength at failure, $\overline{s_{u,mob}}$, defined as:

$$\overline{s_{u,mob}} = \frac{\int_{vol} \Delta\gamma \cdot s_u \, dV}{\int_{vol} \Delta\gamma \, dV} \qquad 4$$

where $\Delta\gamma$ is the incremental shear strain, s_u is the undrained strength in each element of soil within the deformation mechanism and the integration is performed over the volume of the analysis domain. At failure under constant load, only plastic strain increments contribute to the integral, with elastic components being zero. Then, using this value we redefine the vertical bearing capacity factor, N_{cV}, as:

$$N_{cV} = \frac{V_u}{B\overline{s_{u,mob}}} \quad 5$$

For horizontal and moment loading we can define similar capacity factors as follows:

$$N_{cH} = \frac{H_u}{B\overline{s_{u,mob}}} \quad 6$$

$$N_{cM} = \frac{M_u}{B^2\overline{s_{u,mob}}} \quad 7$$

where $\overline{s_{u,mob}}$ is evaluated for failure under the corresponding mode of loading.

If the change in strength dominates the variation in bearing capacity then the capacity factors calculated using the mobilised strength in this way will not change for different magnitudes or durations of preload. Alternatively, if any change in mechanism in itself has a significant effect on the capacity, the bearing capacity factors calculated using Equations 5-7 will vary.

FINITE ELEMENT ANALYSES

Parameters and analysis setup

Small-strain finite element analyses were performed using the Modified Cam Clay (MCC) model in ABAQUS, assuming a plane strain footing of width, *B*, of 1m, and rough interface conditions. Simple, first-order reduced integration coupled pore-fluid-effective stress

elements (CPE4RP) were used in the analyses with a single locally-refined mesh for all cases (Figure 1). The soil parameters are given in Table 1.

The soil was K_0 normally consolidated, with K_0 taken as:

$$K_0 = 1 - \sin\phi_{tc} \approx 0.6 \qquad 8$$

where ϕ_{tc} is the friction angle for triaxial compression. The initial size of the MCC yield envelope can be determined as:

$$p_c^{'} = \frac{q_0^2}{M^2 p_0^{'}} + p_0^{'} \text{ with } M = \frac{6\sin\phi_{tc}}{3 - \sin\phi_{tc}} \qquad 9$$

where $p_0^{'}$ and q_0 are the initial mean effective stress and deviatoric stress, respectively. The initial voids ratio is calculated as:

$$e_0 = e_N - \kappa \ln p_0^{'} - (\lambda - \kappa) \ln p_c^{'} \qquad 10$$

where:

$$e_N = e_{cs} + (\lambda - \kappa)\ln(2) \qquad 11$$

and λ and κ are the compression and swelling indices.

For plane strain conditions the initial undrained strength is calculated following Wroth (1984):

$$s_u = \frac{2}{\sqrt{3}} \cdot \frac{\sin\phi_{tc}}{2a} \cdot \left(\frac{a^2 + 1}{2}\right)^{\Lambda} \sigma_{v0}^{'} \qquad 12$$

where:

$$a = \frac{3 - \sin\phi_{tc}}{2\left(3 - 2\sin\phi_{tc}\right)} \qquad 13$$

and:

$$\Lambda = \frac{\lambda - \kappa}{\lambda} \qquad 14$$

Different levels of uniform stress were applied across the surface of the model to initialise the strength profile. Values were selected to generate dimensionless strength profiles, kB/s_{um}, of approximately 0.4, 2 and 4, which yield undrained strengths at the mudline, s_{um}, of 5.0, 1.0 and 0.5 kPa and a gradient of strength with depth, k, of 2.0 kPa.

Benchmarking for pure *V*, *H* and *M* loading

Pure vertical, horizontal and moment loading analyses were first run with no maintained preload period and loading applied sufficiently quickly that negligible drainage occurred. At the onset of failure for each soil profile, the vertical bearing capacity factors were no more than 8% higher than the equivalent Tresca analyses of Gourvenec and Randolph (2003)[1]. For the horizontal and moment loading the discrepancy was slightly larger but still less than 20% for all cases. These discrepancies are consistent with other coupled analyses of penetrometer penetration by Mahmoodzadeh et al. (2015), where ~9-12% more resistance was generated by the coupled MCC model compared to equivalent total stress approaches using the Tresca model. Even though loading is applied in the simulations sufficiently quickly that negligible drainage occurred it is inevitable that some local redistribution of excess pore pressures will lead to localised increases in strength during the loading process, particularly at the corners of the foundation where the drainage paths are shortest (Mahmoodzadeh et al. 2015).

[1] Linearly interpolating between the published bearing capacity factor values where necessary for kB/s_{um} not analysed in the original paper.

Further mesh refinement (e.g. finer meshes or fanned meshes with smaller elements at the corners of the foundation) could lead to a modest reduction in these discrepancies, which would be expected to yield the greatest improvement for the horizontal loading case (which shows the largest discrepancy compared to the Tresca SSFE analyses of Gourvenec and Randolph, 2003) because the surface element largely controls the capacity at failure. However, the focus of this note is not the absolute bearing capacity but the changes in bearing capacity and failure mechanism, so, accepting these reservations, we have used the mesh shown in Figure 1 for all subsequent analyses.

Parametric analysis for V, V_p-H and V_p-M cases

Additional analyses with preload ratios (V_p/V_u) over the range of 0.1-0.7 at intervals of 0.1 were then modelled, with time periods that allowed all excess pore pressures to dissipate. The consolidated undrained strength was calculated for each element in the finite element analysis mesh as:

$$s_{u,cons} = s_u \exp\left(\frac{e_0 - e_{cons}}{\lambda}\right) \quad 15$$

where e_{cons} is the consolidated voids ratio, which can be calculated as:

$$e_{cons} = \left(\left(1+e_0\right)\cdot\left(1+\varepsilon_v\right)\right)-1 \quad 16$$

where ε_v is the volumetric strain.

The foundation was then loaded to failure by applying further vertical, horizontal or rotational displacement at the centre of the footing, with no constraint on all other degrees of freedom. For the horizontal and moment loading cases the vertical preload was maintained throughout, thereby simulating the self-weight of the foundation. The average mobilised undrained strength, $\overline{s_{u,mob}}$, was calculated for each analysis at the ultimate failure load for the final increment of displacement using Equations 4, 12, 15 and 16, using the spatially-varying consolidated undrained strength, $s_{u,cons}$, for the cases where a maintained preload was applied (i.e. $V_p/V_u > 0.0$). Alternative bearing capacity factors were then calculated using Equations 5-7 and the values of $\overline{s_{u,mob}}$ back-calculated for each analysis.

Figures 2, 3 and 4 show the results of the analyses for all three strength profiles with the applied loads normalised by (i) the in-situ undrained strength at the mudline, s_{um}, and (ii) the average mobilised undrained strength at failure, $\overline{s_{u,mob}}$, for vertical, horizontal and moment loading, respectively. For all loading modes the simulations are compared to bearing capacity

factors derived from small strain FE simulations for strip foundations on Tresca soil published by Gourvenec and Randolph (2003)[2].

The bearing capacity factors for all failure modes and soil profiles collapse to approximately constant values close to the capacity factor for uniform conditions (kB/s_{um} = 0.0), irrespective of the preload ratio applied. Scrutinising the incremental shear strain fields ($\Delta\gamma$) at failure indicated that this convergence towards a constant bearing capacity factor – when the applied loads are normalised by $\overline{s_{u,mob}}$ – occurs even when the failure mechanism visibly changes shape as a result of the preload period and localised changes in soil strength due to consolidation. This is best illustrated in Figure 5, which presents the instantaneous velocity fields at failure for all of the vertical bearing capacity analyses. The mechanisms vary both with strength profile and applied preload. However, the bearing capacity factor N_{cV} is approximately constant when calculated using the mobilised strength $\overline{s_{u-mob}}$ as in Equation 5, rather than the mudline strength s_{um} as defined in Equation 1. In other words, the change in form of the mechanism has an insignificant influence on the bearing capacity factor as defined herein using the average mobilised undrained strength, $\overline{s_{u,mob}}$, rather than using an in-situ strength at a particular depth (typically the mudline).

This observation is important. It means that the proportional increase in $\overline{s_{u,mob}}$ is also the factor by which the bearing capacity increases for a given level of consolidation: changes in $\overline{s_{u,mob}}$ give proportional changes in bearing capacity. Therefore, if this change in strength can be predicted in a simple way for a given initial strength profile, foundation shape, and preload period, it can then be applied to the unconsolidated capacity calculated using standard bearing capacity factors relevant to the initial strength profile. This observation also has parallels with prediction of the pre-failure load-deformation response: changes in the soil stress-strain curve can be scaled into similar changes in load-displacement response, without considering any

[2]Linearly interpolating between the values of kB/s_{um} published by Gourvenec and Randolph (2003).

change in the deformation mechanism (Osman & Bolton 2005, McMahon et al. 2013, Madabhushi & Haigh, 2015).

Ratios of consolidated to unconsolidated average mobilised undrained strength $\left(\overline{s_{u,mob,cons}}/\overline{s_{u,mob}}\right)$ and subsequently the consolidated to unconsolidated bearing capacity factors $\left(N_{cV,cons}/N_{cV};\ N_{cH,cons}/N_{cH};\ N_{cM,cons}/N_{cM}\right)$ were derived for each strength profile modelled and are presented in Figure 6. For all loading types the change in average mobilised undrained strength, $\overline{s_{u,mob}}$, accounts almost completely for the change in foundation capacity as the bearing capacity factors back-calculated are all within ±2% of the value obtained for the analysis with no maintained preload period.

Simple prediction model

There is a linear relationship between preload, V_p/B, and gain in $\overline{s_{u,mob}}$, which is amenable to modelling using the following relationship proposed by Gourvenec et al. (2014) and Feng and Gourvenec (2015):

$$\Delta\overline{s_{u,mob}} = f_\sigma f_{s_u} R\left(\frac{V_p}{B}\right) \qquad 17$$

where R is the normally consolidated undrained strength ratio of the soil (i.e. s_u/σ'_{v0}; 0.29 in this instance) and $f_\sigma f_{s_u}$ is a scaling parameter accounting for the non-uniform distributions of stress and strength gain beneath the foundation as a result of the preloading (in over-consolidated conditions, the scaling is separated into two components, hence the pair of f parameters). This approach can then be used to determine the ratio of consolidated to unconsolidated capacity for different preload ratios, as follows:

$$\frac{V_{u,cons}}{V_u}, \frac{H_{u,cons}}{H_u}, \frac{M_{u,cons}}{M_u} = 1 + \frac{\Delta\overline{s_{u.mob}}}{\overline{s_{u.mob\left(V_p/V_u=0\right)}}} \qquad 18$$

A best fit to the strength gain modelled in the vertical loading analyses was achieved using a constant value of $f_\sigma f_{s_u}$ of 0.4, which is close to the value of 0.36 (f_σ = 0.8 & f_{s_u} = 0.45 $\therefore$ $f_\sigma f_{s_u}$ = 0.36) found by Gourvenec et al. (2014) for a plane strain surface foundation and slightly less than the value of 0.45 found by Chatterjee et al. (2014) for a plane strain pipeline.

Similarly, best fits were achieved for the horizontal loading analyses using a constant value of $f_\sigma f_{s_u}$ of 0.7. This is less than the value of 0.919 found by Feng and Gourvenec for a rectangular mudmat with length to width ratio (L/B) equal to 2 on normally consolidated soil. This reflects that the stress and strength gain distributions beneath a plane strain foundation differ to those that occur beneath a three-dimensional foundation.

Conversely for the moment loading analyses, best fits were achieved with values of 0.55, 0.46 and 0.4 for the soil profiles with kB/s_{um} of 0.4, 2 and 4, respectively. This trend is in general agreement with Feng and Gourvenec's (2016) 3D simulations of a rectangular mudmat foundation (with L/B = 2) for kB/s_{um} of 1.86 and 3.72 (dependent on the orientation of loading). Their best fits across the same range of preload ratio were $f_\sigma f_{s_u}$ of 0.538 and 0.345, respectively.

The performance of Equation 18 in predicting the vertical, horizontal and moment capacities for preload ratios, V_p/V_u, in the range of 0.1 to 0.7 (adopting the $f_\sigma f_{s_u}$ values outlined in the previous paragraphs) is illustrated in Figure 7. The differences between the model predictions and the capacities yielded in the finite element simulations are generally less than 5%.

It appears that appropriate values of $f_\sigma f_{s_u}$ for this simple model vary slightly with geometry (i.e. plane strain foundation, rectangular foundation or plane strain pipeline) and in the case of moment loading are dependent on the initial soil profile (kB/s_{um}). However, in all cases the

changes in soil strength controls the increase in capacity for vertical, horizontal and moment loading, and not any change in failure mechanism. This gain is readily predictable using Equations 17 and 18 when the bearing capacity factor is defined using Equations 5-7.

CONCLUSIONS

This study has separated the effects of strength gain and changes in mechanism on bearing capacity by defining an operative strength explicitly as the average strength mobilised in the failure mechanism. This allows N_c to be defined as a purely geometric quantity, which allows any change in bearing capacity associated with a change in failure mechanism to be identified.

The results indicate that although the failure mechanism may change – via the shear zones and slip planes migrating to preferential locations – this leads to minimal changes in N_{cV}, N_{cH} or N_{cM}. Instead, the gain in capacity is almost entirely due to changes in s_u mobilised within the mechanism. This observation should encourage future studies into consolidated bearing capacity to present gains in capacity in terms of changes in mobilised strength rather than changes in bearing capacity factors.

ACKNOWLEDGEMENTS

This work forms part of the activities of the Centre for Offshore Foundation Systems (COFS), supported as a node of the Australian Research Council's Centre of Excellence for Geotechnical Science and Engineering (CE110001009), and the Industrial Transformation Research Hub in Offshore Floating Facilities, supported by Shell, Woodside, Lloyds Register and Bureau Veritas (ARC grant IH140100012). The second author is supported by the Shell EMI Chair in Offshore Engineering at UWA. This support is gratefully acknowledged.

NOMENCLATURE

a	critical state model parameter
B	foundation width
e_0	initial void ratio
e_{cons}	consolidated voids ratio
e_{cs}	void ratio on critical state line at p'=1kPa
e_N	void ratio on normal consolidation line at p'=1kPa
f_σ	scaling parameter for non-uniform distribution of stress
f_{su}	scaling parameter for non-uniform distribution of strength gain
H_u	ultimate horizontal capacity
K_0	earth pressure coefficient at rest
k	gradient of strength with depth
M	critical state strength parameter
M_u	ultimate moment capacity
$N_{c,H}$	bearing capacity factor for horizontal loading
$N_{c,M}$	bearing capacity factor for moment loading
$N_{c,V}$	bearing capacity factor for vertical loading
p_0'	initial mean effective stress
p_c'	mean effective stress during consolidation
q_0	initial deviatoric stress
s_u	undrained shear strength
$s_{u,cons}$	consolidated undrained shear strength
s_{um}	undrained shear strength at mudline
$\overline{s_{u,mob}}$	mobilised undrained strength
$\overline{s_{u,mob,cons}}$	consolidated mobilised undrained strength
V	volume
V_u	ultimate vertical load
V_p	vertical preload

$\Delta\gamma$	incremental shear strain
ε_v	volumetric strain
$\gamma_c^{'}$	effective unit weight
ϕ_{tc}	friction angle for triaxial compression
κ	slope of swelling line
Λ	plastic compression ratio
λ	slope of normal consolidation line
v	Poisson ratio
$\sigma_{v0}^{'}$	effective vertical stress

REFERENCES

Bienen, B. & Cassidy, M.J. (2013). Setup and resulting punch-through risk of jack-up spudcans during installation. Journal of Geotechnical and Geoenvironmental Engineering, 139(12): 2048-2059.

Bransby, M.F., (2002). The undrained inclined load capacity of shallow foundations after consolidation under vertical loads. In Numerical models in geomechanics: proceedings of the 8th international symposium (NUMOG VIII) (eds. G.N. Pande and S. Pietruszczak), pp. 431-437. Rotterdam, the Netherlands: Balkema.

Chatterjee, S. Gourvenec, S. & White D.J. (2014). Assessment of the consolidated breakout response of partially embedded seabed pipelines. Géotechnique, 64(5): 391-399. doi:10.1680/geot.13.P.215. 64 (5): 391-399.

Feng, X. & Gourvenec, S.M. (2015). Consolidated undrained load-carrying capacity of subsea mudmats under combined loading in six degrees of freedom. Géotechnique, 65(7): 563-575.

Feng, X. & Gourvenec, S. (2016). Modelling sliding resistance of tolerably mobile subsea mudmats. Géotechnique, 66(6):490-499. doi: 10.1680/jgeot.14-15.P.178.

Fu, D., Gaudin, C., Tian, Y., Bienen. B. & Cassidy, M.J. (2015). Effects of preloading with consolidation on undrained bearing capacity of skirted circular footings. Géotechnique, 65(3): 231-246.

Gaone, F.M., Gourvenec, S. & Doherty, J.P. (2017). Large-scale shallow foundation load tests on soft clay - at the National Field Testing Facility (NFTF), Ballina, NSW, Australia. Special issue of Computers in Geotechnics (in press), doi:10.1016/j.compgeo.2017.05.008.

Gourvenec, S.M. & Randolph, M.F. (2003). Effect of strength non-homogeneity on the shape of failure envelopes for combined loading of strip and circular foundations on clay. Géotechnique, 53(6): 575-586.

Gourvenec, S.M., Vulpe, C. & Murthy, T.G. (2014). A method for predicting the consolidated undrained bearing capacity of shallow foundations. Géotechnique, 64(3): 215-225.

Lehane, B.M. & Gaudin, C. (2005). Effects of drained pre-loading on the performance of shallow foundations on over consolidated clay. Proceedings of offshore mechanics and arctic engineering (OMAE), paper OMAE2005-67559.

Lehane, B.M. & Jardine, R.J. (2003). Effects of long-term preloading on the performance of a footing on clay. Géotechnique, 53(8): 689-695.

Madabhushi, S.S.C. & Haigh, S.K. (2015). Investigating the changing deformation mechanism beneath shallow foundations. Géotechnique, 65(8): 684-693.

McMahon, B., Haigh, S.K. & Bolton, M.D. (2013). Optimal displacement mechanisms beneath shallow foundations on linear-elastic perfectly plastic soil. Géotechnique, 63(16): 1447-1450.

Mahmoodzadeh, H., Wang, D. & Randolph, M. F. (2015). Interpretation of piezoball dissipation testing in clay. Géotechnique 65, No. 10, 831-842.

Osman, A. S. & Bolton, M. D. (2005). Simple plasticity-based prediction of the undrained settlement of shallow circular foundations on clay. Géotechnique 55(6): 435–447.

Stanier, S.A., Ragni, R., Bienen, B. & Cassidy, M.J. (2014). Observing the effect of sustained loading on spudcans in clay. Géotechnique, 64(11): 918-926.

Stewart, D. P. (1992). Lateral loading of piled bridge abutments due to embankment construction. PhD thesis, The University of Western Australia, Crawley, Australia.

Vulpe, C., Gourvenec, S. & Cornelius, A. (2016a). Effect of embedment on consolidated undrained capacity of skirted circular foundations in soft clay under planar loading. Canadian Geotechnical Journal, 54(2), pp. 158-172. doi:10.1139/cgj-2016-0265).

Vulpe, C., Gourvenec, S. Leman, B. & Fung, K.N. (2016b). Failure envelopes for consolidated undrained capacity of strip and circular surface foundations. ASCE Journal of Geotechnical and Geoenvironmental Engineering, 142(8): doi:10.1061/(ASCE)GT.1943-5606.0001498.

Vulpe, C, White, D.J. (2014). Effect of prior loading cycles on vertical bearing capacity of clay. International Journal of Physical Modelling in Geotechnics, 14(4): 88-98.

Wroth, C.P. (1984). The interpretation of in situ soil tests. Géotechnique, 34(4): 449-489.

Zdravkovic, L., Potts, D.M. & Jackson, C. (2003). Numerical study of the effect of preloading on undrained bearing capacity. International Journal of Geomechanics. ASCE, 3(1): 1-10.

FIGURES

Figure 1: Schematic of plane strain shallow foundation problem and finite element analysis mesh.

Figure 2: Vertical bearing capacity (conventional normalisation, alternative normalisation): (a,b) kB/s_{um} = 0.4; (c,d) kB/s_{um} = 2.0; and (e,f) kB/s_{um} = 4.0.

Figure 3: Horizontal bearing capacity (conventional normalisation, alternative normalisation): (a,b) kB/s_{um} = 0.4; (c,d) kB/s_{um} = 2.0; and (e,f) kB/s_{um} = 4.0.

Figure 4: Moment bearing capacity (conventional normalisation, alternative normalisation): (a,b) kB/s_{um} = 0.4; (c,d) kB/s_{um} = 2.0; and (e,f) kB/s_{um} = 4.0.

Figure 5: Instantaneous velocity fields at failure for vertical bearing mechanisms, which all result in approximately constant N_{cV} when calculated using the mobilised strength $\overline{s_{u-mob}}$ as in Equation 5, rather than the mudline strength s_{um} as in Equation 1.

Figure 6: Comparison of relative importance of strength and mechanism changes for: (a) vertical bearing capacity; (b) horizontal bearing capacity; and (c) moment bearing capacity.

Figure 7: Comparison of simulated and predicted capacity for preloads, V_p/V_u, in the range of 0-0.7 and κ (= kB/s_{um}) of 0.4, 2.0 and 4.0: (a) vertical loading; (b) horizontal loading; and (c) moment loading.

LIST OF TABLES

Table 1: Modified Cam Clay parameters for UWA Kaolin clay (after Stewart, 1992).

FIGURES

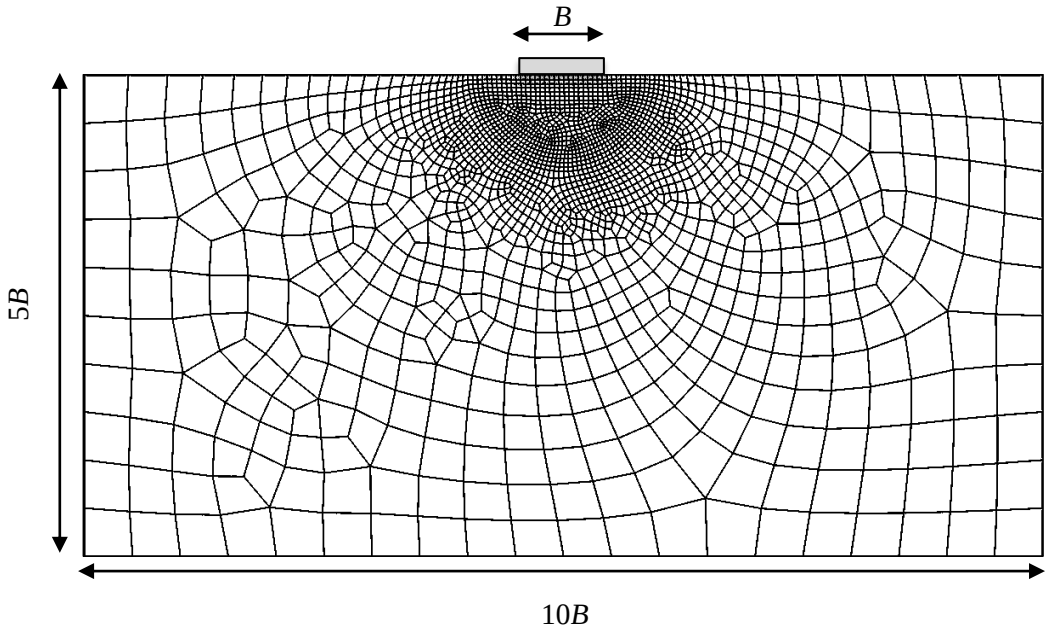

Figure 2: Schematic of plane strain shallow foundation problem and finite element analysis mesh.

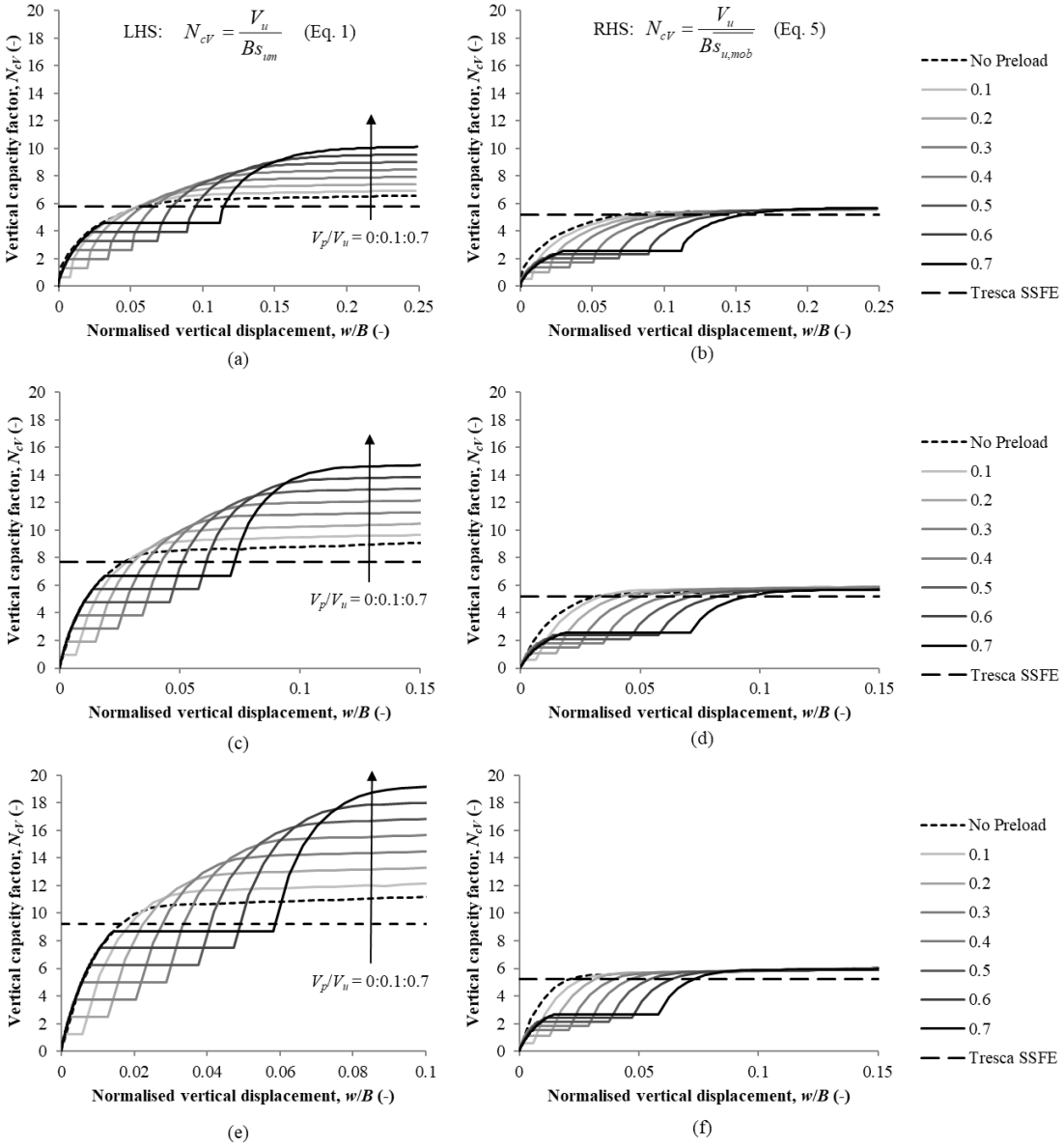

Figure 2: Vertical bearing capacity (conventional normalisation, alternative normalisation):

(a,b) kB/s_{um} = 0.4; (c,d) kB/s_{um} = 2.0; and (e,f) kB/s_{um} = 4.0.

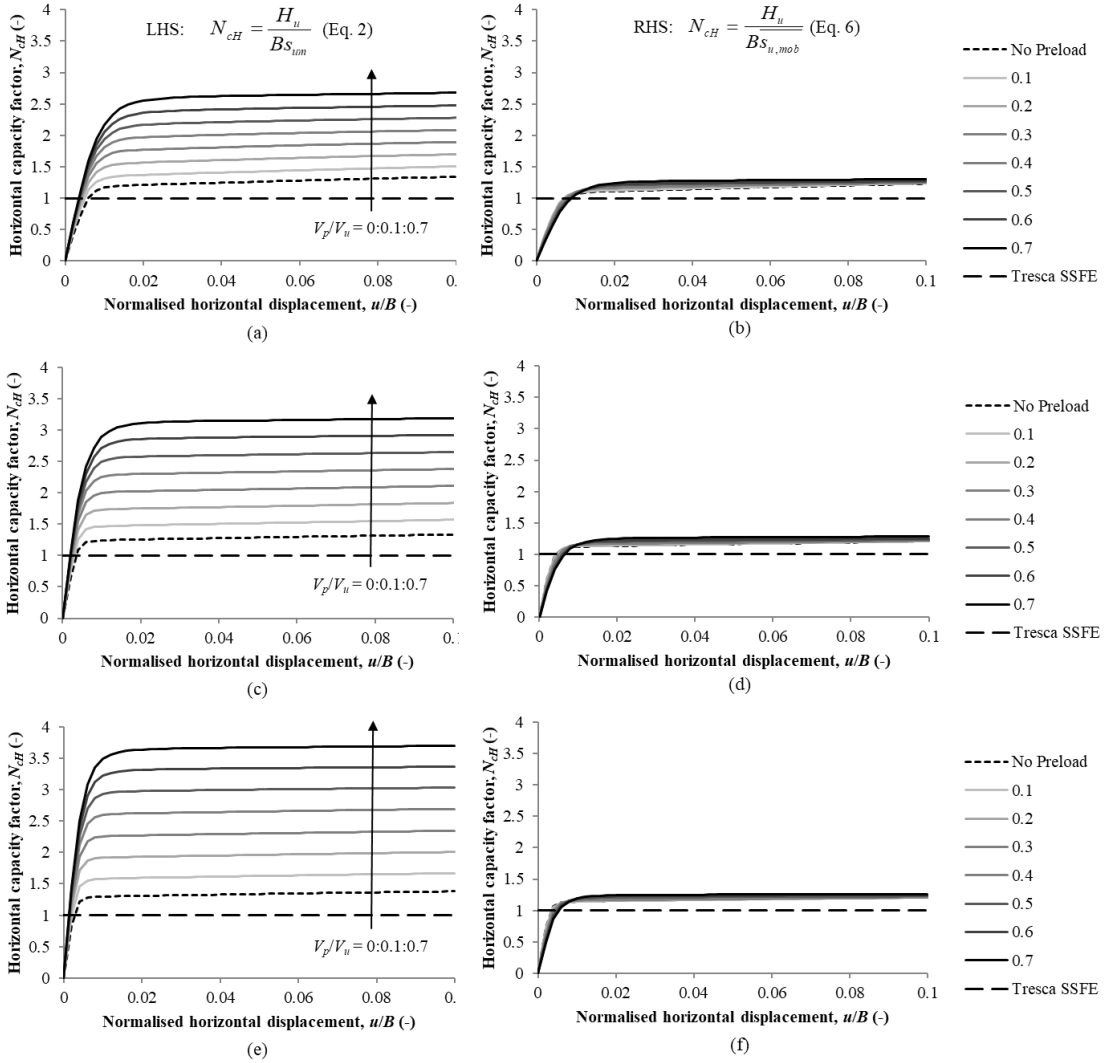

Figure 3: Horizontal bearing capacity (conventional normalisation, alternative normalisation):

(a,b) kB/s_{um} = 0.4; (c,d) kB/s_{um} = 2.0; and (e,f) kB/s_{um} = 4.0.

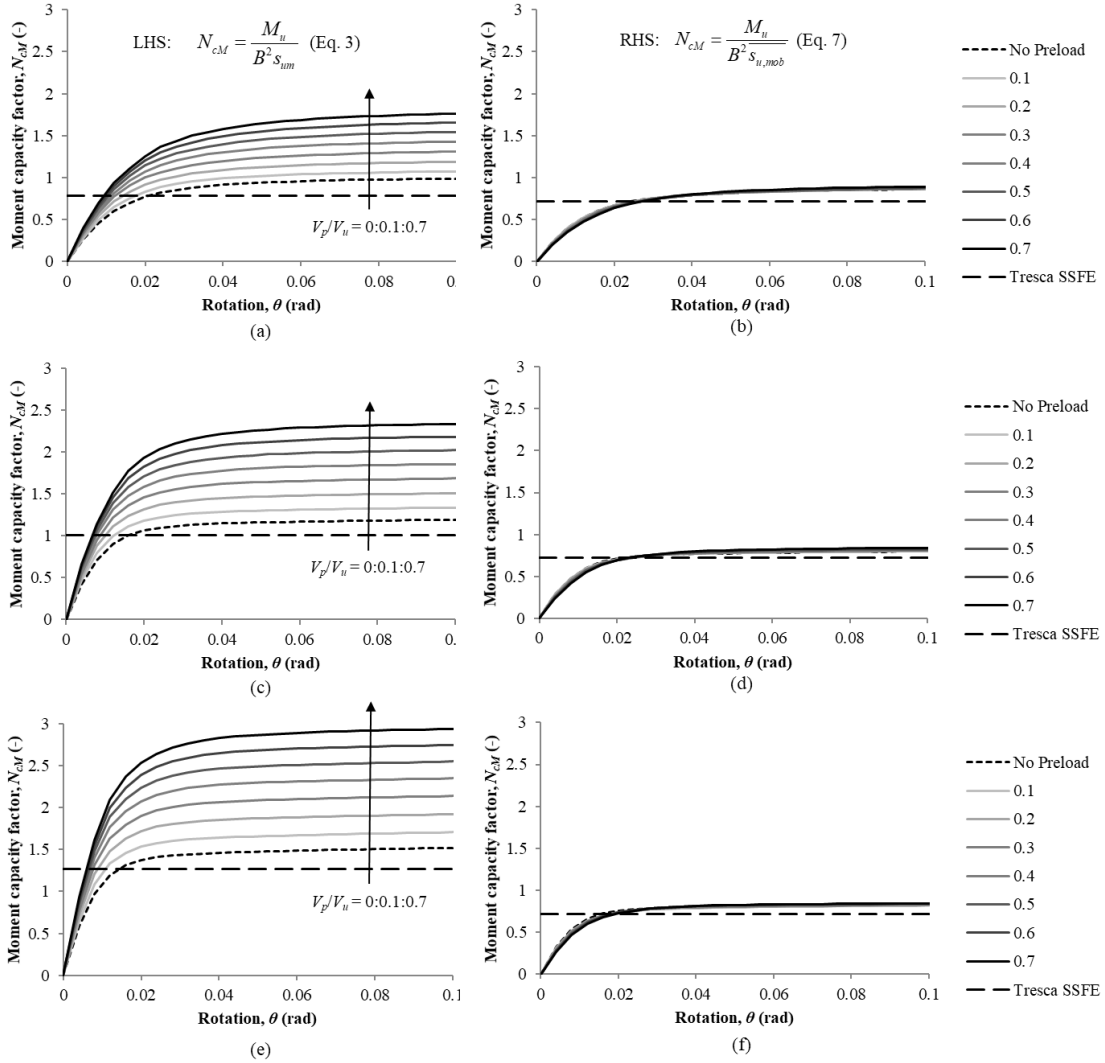

Figure 4: Moment bearing capacity (conventional normalisation, alternative normalisation):

(a,b) kB/s_{um} = 0.4; (c,d) kB/s_{um} = 2.0; and (e,f) kB/s_{um} = 4.0.

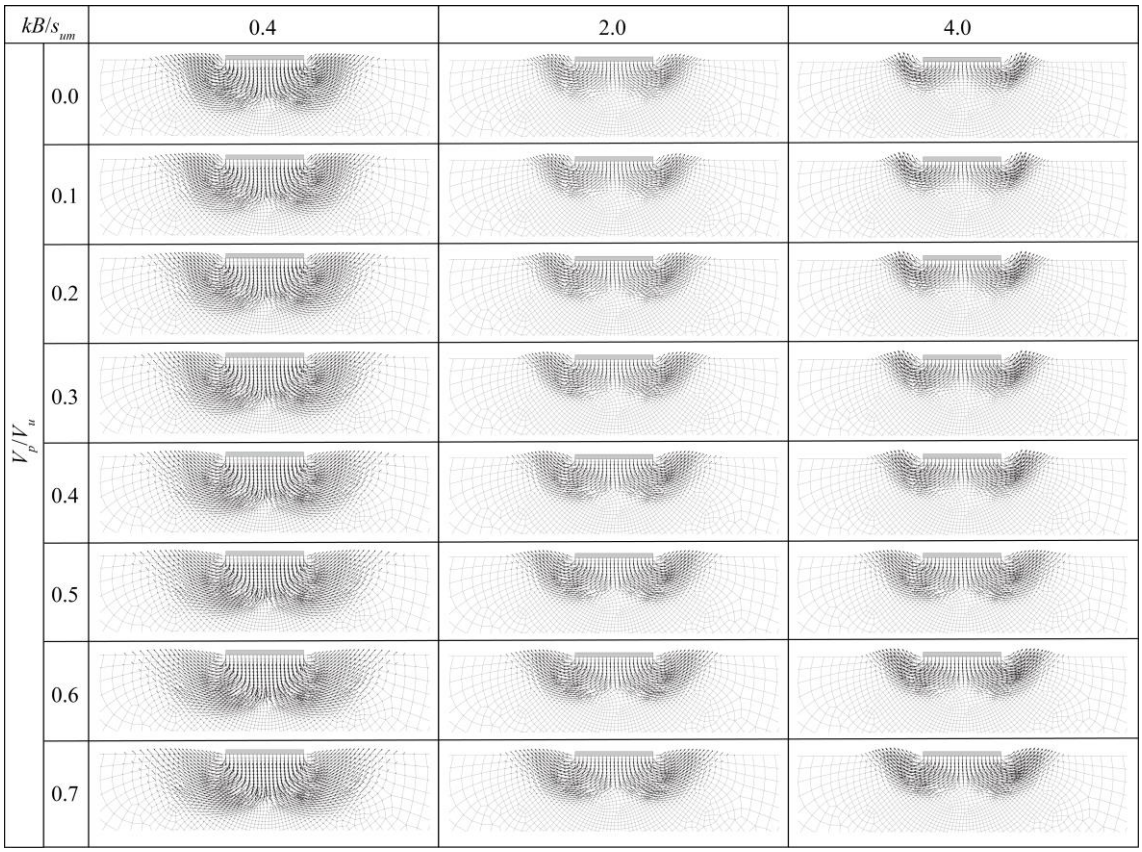

Figure 5: Instantaneous velocity fields at failure for vertical bearing mechanisms, which all result in approximately constant N_{cV} when calculated using the mobilised strength $\overline{s_{u-mob}}$ as in Equation 5, rather than the mudline strength s_{um} as in Equation 1.

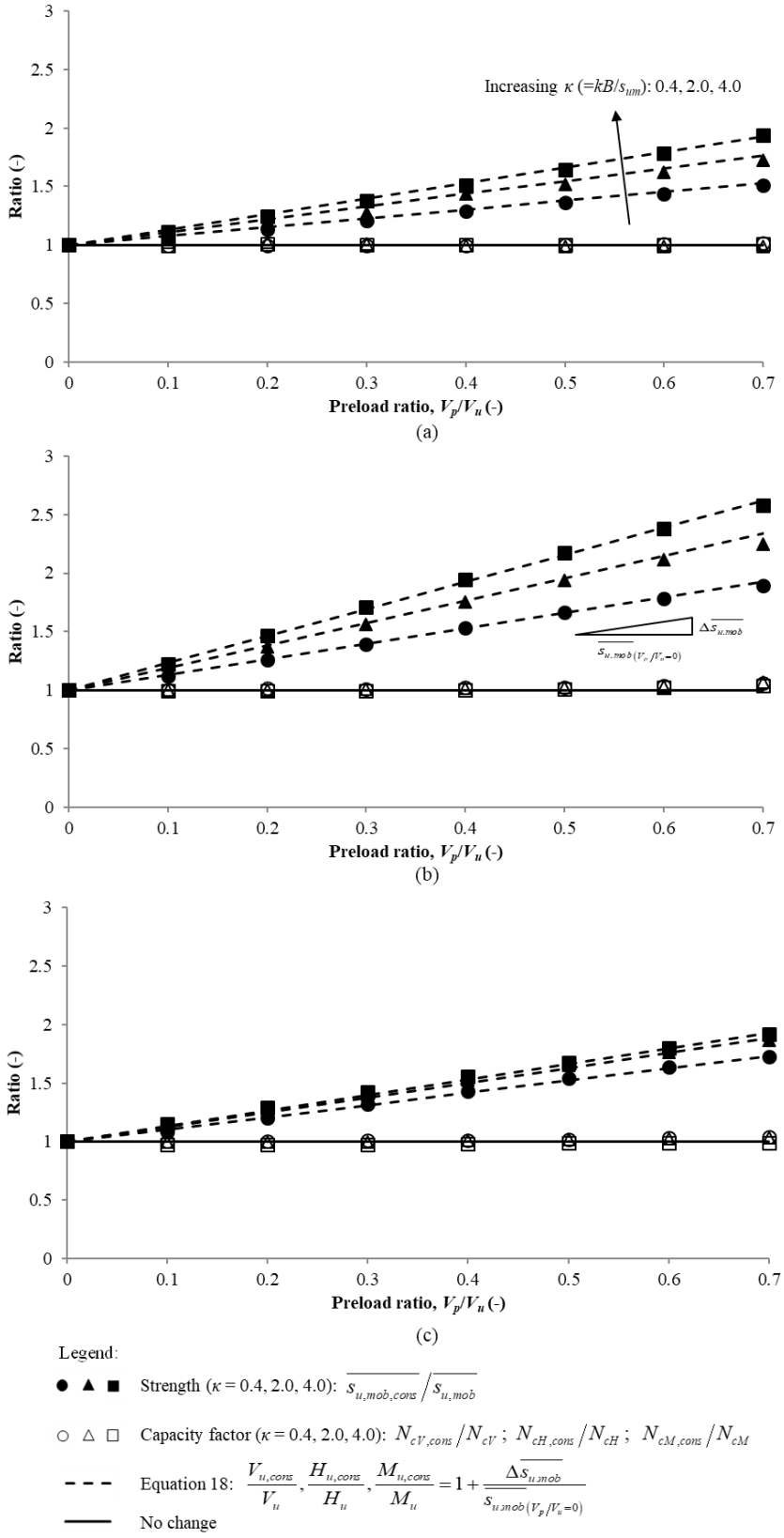

Figure 6: Comparison of relative importance of strength and mechanism changes for: (a) vertical bearing capacity; (b) horizontal bearing capacity; and (c) moment bearing capacity.

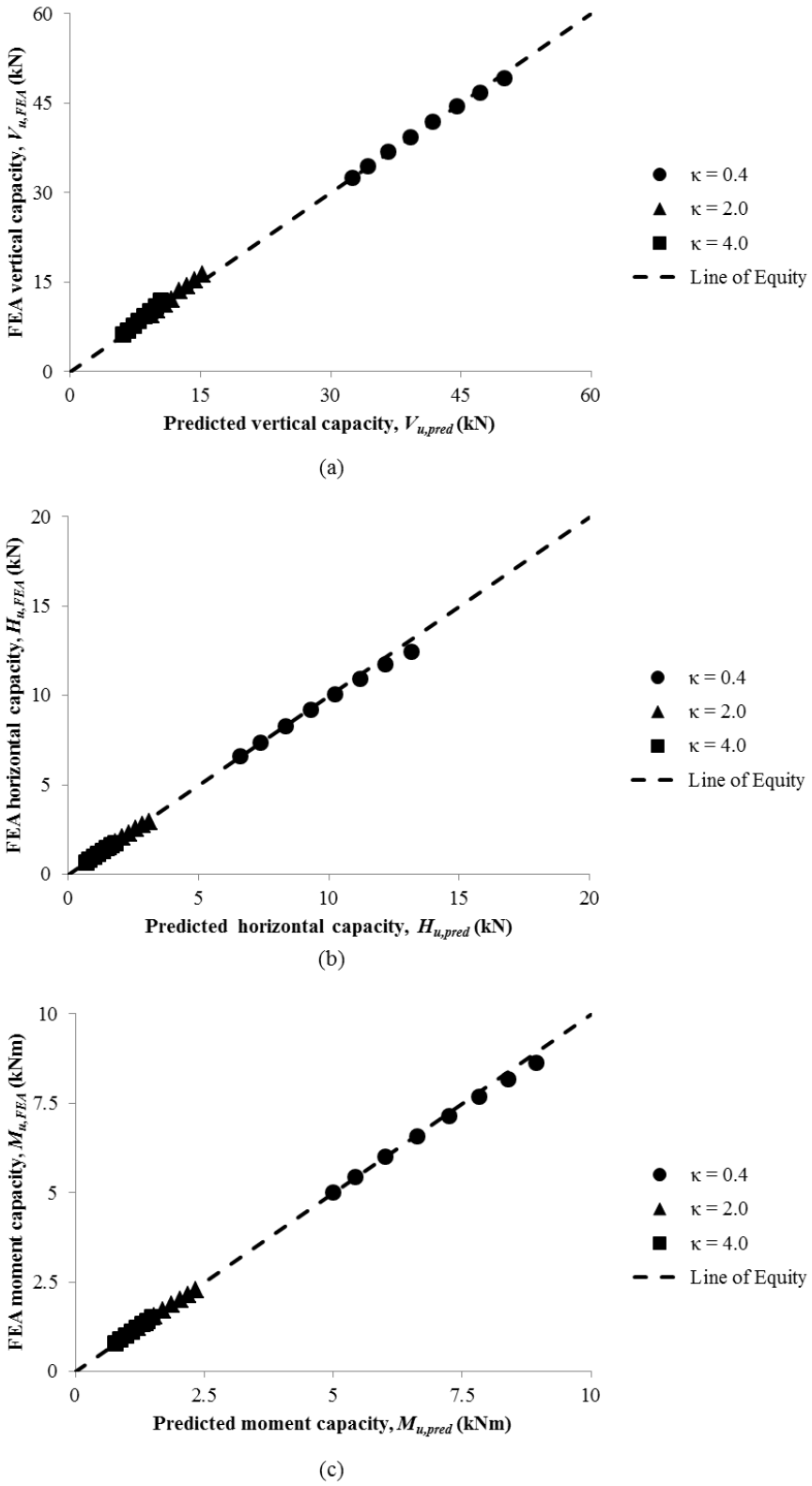

Figure 7: Comparison of simulated and predicted capacity for preloads, V_p/V_u, in the range of 0-0.7 and κ (= kB/s_{um}) of 0.4, 2.0 and 4.0: (a) vertical loading; (b) horizontal loading; and (c) moment loading.

TABLES

Table 1: Modified Cam Clay parameters for UWA Kaolin clay (after Stewart, 1992).

Critical state friction angle for triaxial compression, ϕ_{tc} (°)	23.5
Void ratio at p' = 1 kPa on CSL, e_{cs} (-)	2.14
Slope of normal compression line in e-ln p' space, λ (-)	0.205
Slope of recompression line in e-ln p' space, κ (-)	0.044
Poisson's ratio, υ (-)	0.3
Effective unit weight, γ_c' (kN/m^3)	7
Permeability, k (m/s)	1×10^{-9}